JOURNAL OF Materials CHEMISTRY

High pressure synthesis, crystal structure and physical properties of a new Ni(II) perovskite $BiNiO_3$

Shintaro Ishiwata,*[a] Masaki Azuma,[a,b] Mikio Takano,[a] Eiji Nishibori,[c] Masaki Takata,[c] Makoto Sakata[c] and Kenichi Kato[d]

[a]*Institute for Chemical Research, Kyoto University, Uji, Kyoto-fu 611-0011, Japan. E-mail: ishi@msk.kuicr.kyoto-u.ac.jp*
[b]*PRESTO, Japan Science and Technology Corporation (JST), Kawaguchi, Saitama 332-0012, Japan*
[c]*Department of Applied Physics, Nagoya University, Chigusa-ku, Nagoya 464-8601, Japan*
[d]*Japan Synchrotron Radiation Research Institute (JASRI), 1-1-1 Kouto, Mikazuki-cho, Sayo-gun, Hyogo 679-5198, Japan*

Received 24th June 2002, Accepted 20th September 2002
First published as an Advance Article on the web 15th October 2002

A new triclinic perovskite, $BiNiO_3$, has been synthesized at a high pressure of 6 GPa in an oxidizing atmosphere. Structure refinements based on synchrotron X-ray powder diffraction and bond-valence calculations revealed a disproportionation of the Bi ions into Bi^{3+} and Bi^{5+}, both being located in distorted oxygen octahedra. Because of the presence of Bi^{5+}, the oxidation state of Ni was +2, rather than +3 as had been expected; $BiNiO_3$ thus showed insulating behavior with localized spins of $S = 1$.

Introduction

$MNiO_3$ perovskites (M = rare earth element or Tl) have attracted much attention because of their metal (high temperature phase)–insulator (low temperature phase) (MI) transition which changes systematically as a function of structural features.[1–4] The transition temperature (T_{MI}) increases monotonically as the M ion becomes smaller, or as the tolerance factor becomes smaller, suggesting that the relevant σ* band, composed of Ni 3d and O 2p orbitals, becomes narrower as the Ni–O–Ni bond angle decreases.[5] However, the systematics concerning the electronic structure in the insulating phase are rather complicated. Neutron diffraction studies have revealed that a charge disproportionation to $Ni^{(3+\delta)+}$ and $Ni^{(3-\delta)+}$, associated with an orthorhombic to monoclinic structural change, takes place at T_{MI} for M = Lu, Yb, Tm, Er, and Ho.[6–8] According to X-ray and neutron diffraction studies, there is no such symmetry change for M = Sm, Nd, and Pr, but the lattice volume increases by 0.15–0.25% at T_{MI}.[9] By means of Raman spectroscopy and electron diffraction, however, a monoclinic distortion was found quite recently for $NdNiO_3$.[10] For $PrNiO_3$, another mechanism, orbital ordering, may be the origin of the MI transition.[11] This oxide shows an orthorhombic (metal) to rhombohedral (metal) transition only above 700 K, while $LaNiO_3$ remains rhombohedral and metallic down to 1.5 K.[9,12] In this context, the replacement of La^{3+} with a larger ion, such as Bi^{3+}, could be expected to lead to cubic symmetry and metallicity. Rather than this simple expectation, we considered a more intriguing possibility: the lattice volume might be large enough to make this oxide insulating and, therefore, more interesting from the perspective of spin–orbital coupled physics. From this viewpoint, Ni^{3+} is an interesting species, having the smallest spin of $S = 1/2$ and twofold orbital degeneracy.[13] $BiNiO_3$ has previously been reported to be obtainable at high pressure (HP) with cubic symmetry, but detailed structural data were not presented.[14–16]

In this paper, we report a successful HP synthesis, newly discovered structural features, and also the magnetic and electrical properties of $BiNiO_3$. Contrary to our expectation, this compound has been found to be an insulating antiferromagnet which is heavily distorted to triclinic symmetry ($P\bar{1}$). A precise structural analysis based on a synchrotron radiation X-ray powder diffraction (XRD) study revealed that the Bi ions were disproportionated to Bi^{3+} and Bi^{5+} and, therefore, the oxidation state of Ni ion was +2 rather than the expected +3.

Experimental

Synthesis

The high pressure syntheses of polycrystalline samples of $BiNiO_3$ were carried out from a precursor prepared as follows. Stoichiometric amounts of Bi_2O_3 and Ni were dissolved in nitric acid, stirred, and then heated at 750 °C in the air for 12 h. The fine powders obtained were mixed with $KClO_4$ in a weight ratio of 4 : 1 and were sealed in a gold capsule. The sample was then treated at 6 GPa and 1000 °C for 30 min in a conventional cubic anvil-type high pressure apparatus. It should be noted that the heating rate seriously influenced the quality of the sample. When the temperature was increased slowly, significant amounts of unidentified impurity phases remained in the final product. The amounts of the impurities were lowest when the temperature was increased to 1000 °C in 1 min. After removal from the capsule, the sample was crushed and washed in distilled water to dissolve the KCl. Finally, the remaining solid was dried with acetone. To obtain a sintered pellet for resistivity measurements, the high pressure and high temperature treatment was repeated at 6 GPa and 800 °C for 10 min without mixing with $KClO_4$.

Characterization

Powder XRD data were recorded on a Rigaku RINT 2000 diffractometer using Cu-Kα radiation for phase identification. Synchrotron XRD experiments were carried out using a large Debye–Scherrer camera installed at beam line BL02B2 of SPring-8, Japan Synchrotron Radiation Research Institute, for the structure refinement. The granularity of the powder sample was homogenized to 2–3 μm in diameter by means of a precipitation method. The sample was ground carefully with

ethanol in an agate mortar and then transfered to a Petri dish. The finely ground sample was well mixed with more ethanol and left to stand for 45 min so that the large particles precipitated. The upper half of the suspension was removed, put in another Petri dish, and left for 1.5 h. Then, particles too small for the diffraction study were skimmed from the top of the suspension and the remainder dried at 100 °C for 1 h in an oven. The powder sample thus selected was transferred to a 0.1 mm diameter glass capillary. The homogeneity of the X-ray intensity was confirmed by checking the Debye–Scherrer pattern image recorded on an imaging plate. The diffraction data were collected in 0.01° steps with an incident beam of wavelength $\lambda = 0.55129$ Å at 300 K. The structural parameters were refined by Rietveld analysis of the intensity data in the 2θ range 6.9–40.0° with RIETAN-2000[17] on the basis of space group $P\bar{1}$ (no. 2).

Physical property measurements

Thermogravimetric and differential thermal analyses (TG-DTA) were conducted in an 80% N_2–20% O_2 atmosphere. The sample was heated from 25 to 750 °C at a rate of 5 °C min^{-1}. DC magnetic susceptibility measurements were performed with a Quantum Design MPMS XL SQUID magnetometer in an external magnetic field of 0.1 T between 2 and 400 K on heating after zero-field cooling and then on cooling. Magnetization was measured in the external magnetic fields below 5 T at 5, 200, and 300 K. Electrical resistivity was measured by the dc four-probe method (silver paste contacts) from 350 to 200 K using a Quantum Design PPMS.

Results and discussion

Crystal structure

The powder XRD pattern of $BiNiO_3$ was indexed with a triclinic unit cell [$a = 5.3852(2)$, $b = 5.6498(2)$, $c = 7.7078(3)$ Å, $\alpha = 91.9529(10)$, $\beta = 89.8097(9)$, $\gamma = 91.5411(9)°$]. Since the lattice parameters corresponded to $\sqrt{2}a \times \sqrt{2}a \times 2a$ of a perovskite, the structure refinement was performed assuming a distorted $GdFeO_3$-type structure. Fig. 1 shows the results of the Rietveld analysis. The observed, calculated, and difference patterns, as well as the allowed reflections, are shown in the figure. The data in the ranges 8.4–8.5, 10.6–11.0, and 12.95–13.15° were excluded in the refinement because of the presence of reflections from unidentified impurities. The crystallographic data and the reliability factors are summarized in Table 1. The fit was quite good, as indicated by the R_I and R_F values (1.35 and 0.62%, respectively, for 942 reflections). The oxygen occupancies were fixed to 1 during the refinements. Those of Bi and Ni were also fixed to 1 in the final refinement because these were fully occupied within the standard deviations. Fig. 2 illustrates the refined structure of $BiNiO_3$.

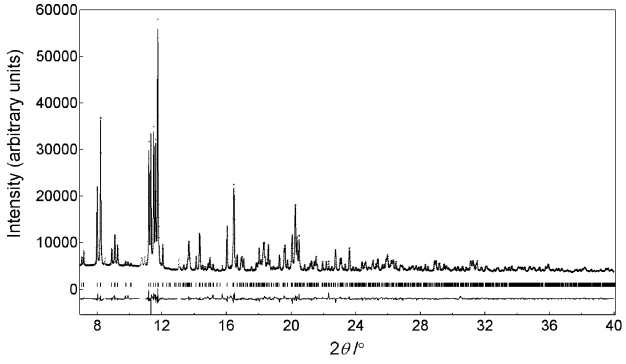

Fig. 1 Observed (+), calculated (solid line), and difference (below) synchrotron powder X-ray diffraction patterns. The tick marks indicate the calculated peak positions.

Table 1 Occupancies, atomic positions, and atomic displacement parameters for $BiNiO_3$[a]

Atom	Site	g	x	y	z	B/Å^2
Bi1	2i	1	0.0065(4)	0.0487(3)	0.2356(2)	0.66(5)
Bi2	2i	1	0.5109(4)	0.4433(3)	0.7259(2)	0.49(5)
Ni1	1d	1	0.5	0	0	0.54(20)
Ni2	1c	1	0	0.5	0	1.26(23)
Ni3	1f	1	0.5	0	0.5	0.89(20)
Ni4	1g	1	0	0.5	0.5	0.86(21)
O1	2i	1	−0.1488(49)	0.4656(37)	0.2551(32)	0.68(21)
O2	2i	1	0.4070(43)	0.0801(35)	0.7607(31)	0.68(21)
O3	2i	1	0.8219(44)	0.1760(36)	−0.0298(29)	0.68(21)
O4	2i	1	0.3236(44)	0.3499(37)	0.0829(31)	0.68(21)
O5	2i	1	0.2203(40)	0.8032(39)	0.4030(28)	0.68(21)
O6	2i	1	0.6551(41)	0.6638(33)	0.5345(32)	0.68(21)

[a] $a = 5.3852$ (2), $b = 5.6498(2)$, $c = 7.7078(3)$ Å, $\alpha = 91.9529(10)$, $\beta = 89.8097(9)$, $\gamma = 91.5411(9)°$, $Z = 4$, $V = 234.29(1)$ Å^3, $R_{wp} = 2.72\%$, $R_p = 1.85\%$, $R_e = 1.36\%$, $S = 2.00$, $R_I = 1.35\%$, $R_F = 0.62\%$.

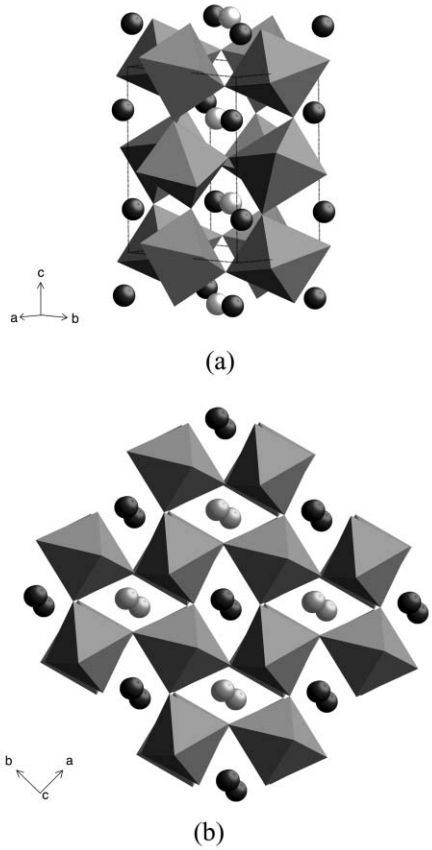

Fig. 2 Crystal structure of $BiNiO_3$ (a) and the projection along the c axis. (b) The dark and light gray spheres correspond to Bi1(+3) and Bi2(+5) ions, respectively. Ni ions are in the octahedra.

Both Bi1 and Bi2 form columns in the c direction. As can be seen from the bond distances and angles summarized in Tables 2 and 3, the degrees of tilting of the NiO_6 octahedra are significantly larger compared to other members of the $MNiO_3$ perovskite series.[1] The Ni–O–Ni bond angles of $BiNiO_3$ are in the range 130.3–144.5°, while even those of $LuNiO_3$ are 143.4–145.1°.[7] Another characteristic is the relatively long Ni–O bond length. The average bond length is 2.09 Å, which is 8% longer than that of $LaNiO_3$.[9] Accordingly, the unit cell volume (234.3 Å^3) is significantly larger than that of 2/3$LaNiO_3$ (226.0 Å^3). This is indicative of low oxidation states for the nickel ions. This was confirmed by the bond-valence calculations[18] summarized in Table 4. The bond-valence sums for Bi1, Bi2, Ni1, Ni2, Ni3, and Ni4 are 2.99, 5.20 1.99, 1.88, 1.98, and 1.71, respectively, indicating that the oxidation states are

Table 2 Selected bond lengths for $BiNiO_3$

Bond	r/Å	Bond	r/Å
Bi1–O3	2.21(2)	Bi2–O1	2.03(3)
Bi1–O5	2.27(2)	Bi2–O4	2.04(2)
Bi1–O2	2.32(2)	Bi2–O6	2.10(2)
Bi1–O3	2.42(2)	Bi2–O2	2.14(2)
Bi1–O1	2.52(2)	Bi2–O5	2.24(2)
Bi1–O4	2.68(2)	Bi2–O6	2.26(3)
Bi1–O6	2.96(2)	Bi2–O4	2.99(2)
Bi1–O5	3.13(2)	Bi2–O3	3.00(2)
Bi1–O2	3.26(2)	Bi2–O1	3.46(2)
Bi1–O1	3.39(2)	Bi2–O3	3.63(2)
Bi1–O4	3.70(2)	Bi2–O5	3.65(3)
Bi1–O6	3.70(2)	Bi2–O2	3.66(4)
Ni1–O2 (×2)	1.98(2)	Ni2–O3 (×2)	2.05(2)
Ni1–O3 (×2)	1.99(3)	Ni2–O4 (×2)	2.07(2)
Ni1–O4 (×2)	2.29(2)	Ni2–O1 (×2)	2.13(2)
Ni3–O5 (×2)	1.98(2)	Ni4–O1 (×2)	2.05(3)
Ni3–O2 (×2)	2.11(2)	Ni4–O6 (×2)	2.11(2)
Ni3–O6 (×2)	2.12(2)	Ni4–O5 (×2)	2.21(2)

Table 3 Selected bond angles for $BiNiO_3$

Bonds	Angle/°	Bonds	Angle/°
O2–Ni1–O3	90.8(9)	O3–Ni2–O4	87.7(8)
O2–Ni1–O4	94.4(9)	O1–Ni2–O3	99.8(9)
O3–Ni1–O4	88.7(8)	O1–Ni2–O4	88.9(10)
O2–Ni3–O5	96.0(6)	O1–Ni4–O6	101.8(9)
O5–Ni3–O6	97.7(9)	O5–Ni4–O6	80.8(7)
O2–Ni3–O6	81.6(8)	O1–Ni4–O5	86.6(9)
Ni4–O1–Ni2	133.9(13)	Ni1–O2–Ni3	140.9(11)
Ni1–O3–Ni2	144.5(9)	Ni2–O4–Ni1	130.3(10)
Ni3–O5–Ni4	133.5(11)	Ni4–O6–Ni3	138.4(9)

Table 4 Bond-valence sums for Bi and Ni calculated from the Bi–O and Ni–O bond lengths shorter than 3.2 Å

	Bi1	Bi2	Ni1	Ni2	Ni3	Ni4
V^a	2.99	5.20	1.99	1.88	1.98	1.71

[a] V is the sum of individual bond valences (s_i) for Bi–O and Ni–O. $s_i = \exp[(r_0 - r_i)/B]$; $B = 0.37$, $r_0 = 2.094$, 2.06, 1.654 for Bi^{3+}–O, Bi^{5+}–O, and Ni^{2+}–O, respectively.

$Bi^{3+}{}_{1/2}Bi^{5+}{}_{1/2}Ni^{2+}O_3$ rather than $Bi^{3+}Ni^{3+}O_3$. The presence of highly oxidized Bi^{5+} resulted in reduction of the Ni oxidation state to +2.

The origin of the strong distortion of this compound will now be discussed. In an ideal perovskite, the A site cation is coordinated by 12 oxygen ions and the coordination number decreases with the degree of distortion. In the present triclinic compound, however, there are discrepancies between the 6th and 7th shortest Bi–O bond lengths for both Bi1 and Bi2. As shown in Fig. 3(a), the six oxygen surrounding Bi1 make octahedra which form edge-sharing dimers parallel to the c axis, as do the Bi2 octahedra. Since the Bi–O bond has a strongly covalent character, Bi ions sometimes occupy the B sites of perovskites, as in $BaBiO_3$, where a disproportionation into Bi^{3+} and Bi^{5+} also occurs.[19] In the case of $BiNiO_3$, both the formation of BiO_6 octahedra and the disproportionation into Bi^{3+} and Bi^{5+} cause the extensive tilting of the NiO_6 octahedra and, thus, the distortion of the whole structure. Judging from the Bi–O and O–O bond lengths, the $6s^2$ lone pairs of Bi1(+3) seem to point in the directions opposite to the shared edge, as shown in Fig. 3(b). Although this seems to be inconsistent with the shifts of Bi1 ions in the octahedra, the centers of the octahedra are too far from the original positions of the Bi ions in the $GeFeO_3$ structure. The repulsion between

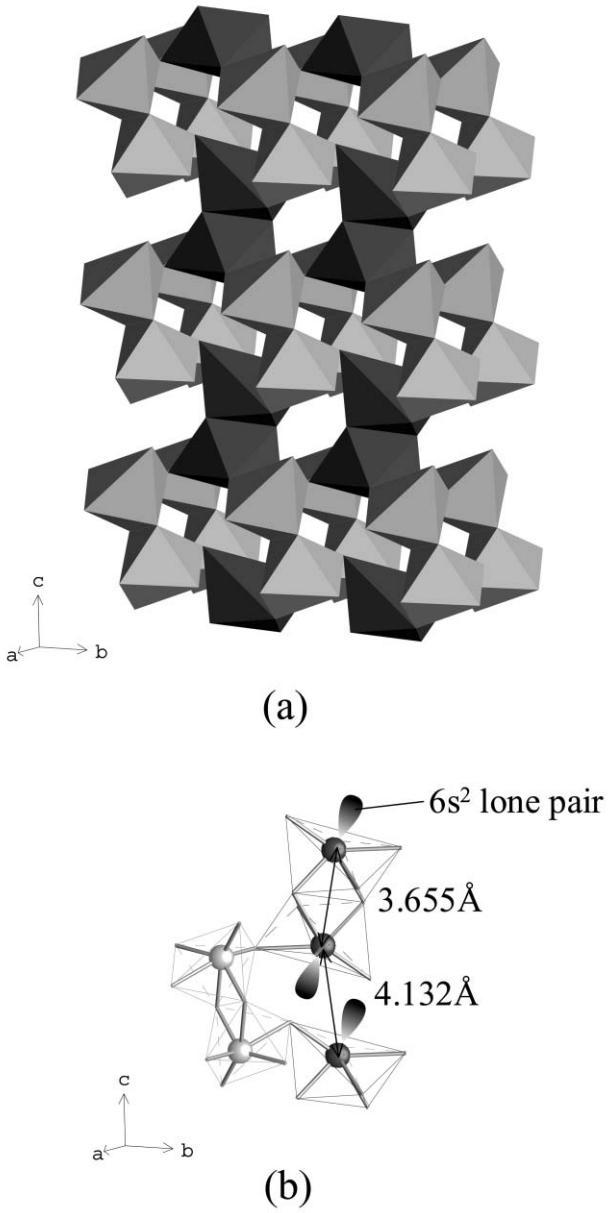

Fig. 3 Linkage of BiO_6 octahedra in $BiNiO_3$. (a) Bi1(+3) and Bi2(+5) ions are shown as dark and light gray octahedra, respectively. (b) The positions of Bi ions and the $6s^2$ lone pairs in the octahedra.

the polarized lone pairs cause the dimerization of Bi1–O octahedra. As far as we know, $BiNiO_3$ provides the first example of the disproportionation of Bi ions in the A site.

Thermal stability

TG and DTA curves for $BiNiO_3$ are shown in Fig. 4. Weight loss owing to the release of oxygen was observed in three steps. The abrupt downturn in the DTA curve at 240 °C indicates that the first oxygen loss, starting at 150 °C, is associated with a structural transition, probably to a higher symmetry. Since the remainder was identified to be a mixture of Bi_2O_3 and NiO by XRD experiments, the decomposition can be expressed as:

$$2BiNiO_3 \rightarrow Bi_2O_3 + 2NiO + 0.5O_2\uparrow$$

The observed weight loss of 2.65% is slightly larger than calculated for $BiNiO_3$ (2.53%), probably due to the presence of unidentified impurities. The further weight loss above 450 °C can be attributed to partial oxygen loss and subsequent sublimation of Bi_2O_3, as found in the case of $TlNiO_3$.[4]

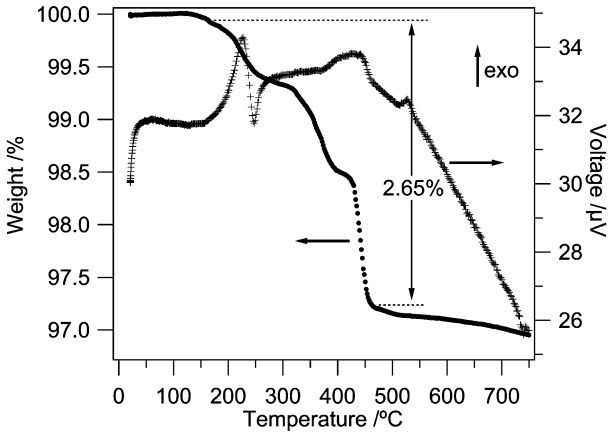

Fig. 4 TG (●) and DTA (+) curves for $BiNiO_3$ measured in 80% N_2–20% O_2 atmosphere with a heating rate of 5 °C min^{-1}.

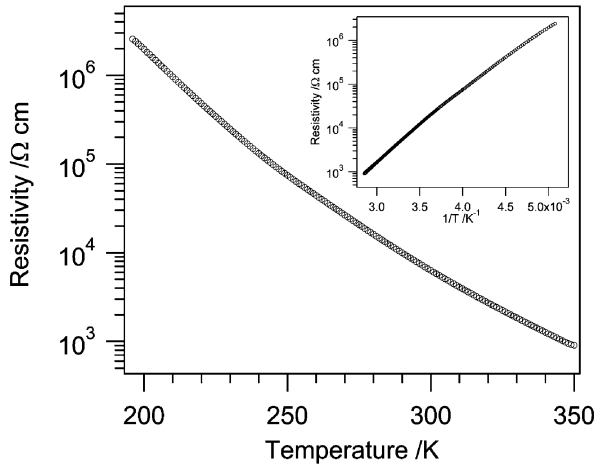

Fig. 5 Temperature dependence of the resistivity for $BiNiO_3$ measured on cooling. The inset shows the Arrhenius plot of the data.

Magnetic and electrical properties

The temperature dependence of the electrical resistivity for $BiNiO_3$ exhibits insulating behavior, as shown in Fig. 5. This is consistent with the above conclusion that the Ni oxidation state is +2 rather than +3. The inset in Fig. 5 shows the Arrhenius plot of the data, from which an excitation energy of 675 meV was estimated.

The temperature dependence of the magnetic susceptibility of $BiNiO_3$ is plotted in Fig. 6(a). The data between 400 and 350 K were fit to the Curie–Weiss law with a temperature-independent term, $\chi(T) = \chi_0 + C/(T - \theta)$, where $\chi_0 = -1.25 \times 10^{-4}$ emu mol^{-1}, $C = 1.05$ emu K mol^{-1} and $\theta = -262$ K. The estimated Curie constant is quite close to that expected for $S = 1$ spins rather than for an $S = 1/2$ system, as clearly shown in the slope of the inverse susceptibility plotted in Fig. 6(b). This fact confirms the divalent nature of Ni, with $S = 1$, as suggested from the structure analysis and the resistivity data. The negative Weiss constant indicates antiferromagnetic interactions between the spins. The system becomes magnetically ordered at 300 K and the data collected on heating and cooling were not coincident below T_N. The ferromagnetic hysteresis can be clearly seen in the M–H data shown in Fig. 7. Since the spin–spin interaction is antiferromagnetic, these ferromagnetic features can be attributed to a weak ferromagnetism owing to the spin canting, reflecting the small Ni–O–Ni bond angles in this compound.

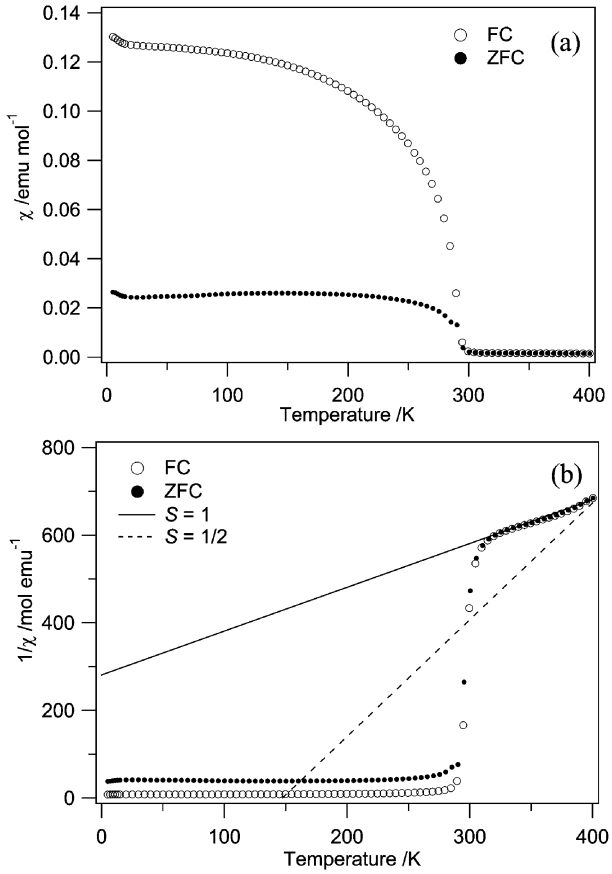

Fig. 6 Temperature dependencies of the molar magnetic susceptibility (a) and inverse molar magnetic susceptibility (b) for $BiNiO_3$ measured in an external magnetic field of 0.1 T on heating after zero-field cooling (ZFC) and then on cooling (FC). The solid and broken lines correspond to the slopes expected for $S = 1$ and $S = 1/2$ systems, respectively.

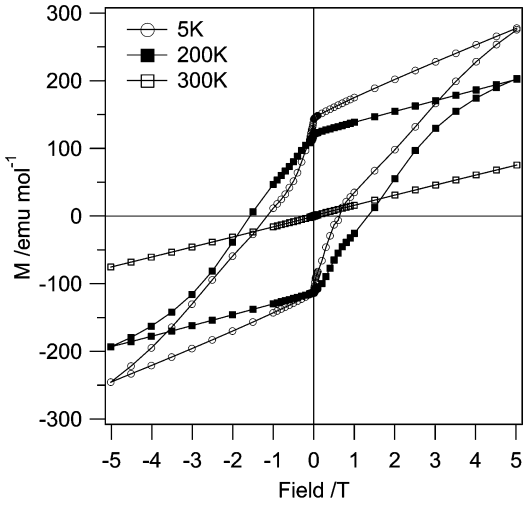

Fig. 7 Magnetization curves of $BiNiO_3$ at 5, 200, and 300 K.

Conclusion

The new triclinic perovskite $BiNiO_3$ was synthesized at a high pressure of 6 GPa in an oxidizing atmosphere. The oxidation state was found to be $Bi^{3+}{}_{1/2}Bi^{5+}{}_{1/2}Ni^{2+}O_3$ rather than $Bi^{3+}Ni^{3+}O_3$. This gives insulating character with localized $S = 1$ moments in the system. Because of the strong covalent character of Bi–O bonds, both Bi^{3+} and Bi^{5+} ions were coordinated in BiO_6 octahedra. The substitution of Bi with other cations might suppress the disproportionation and, thus, lead to metallic conductivity, as in $BaBiO_3$.

Acknowledgements

The synchrotron radiation experiments were performed at the SPring-8 with the approval of the Japan Synchrotron Radiation Research Institute. The authors express their thanks to the Ministry of Education, Culture, Sports, Science and Technology, Japan, for Grants-in-Aid No. 12CE2005, for COE Research on Elements Science, and No. 13440111.

References

1 P. Lacorre, J. B. Torrance, J. Pannetier, A. I. Nazzal, P. W. Wang and T. C. Huang, *J. Solid State Chem.*, 1991, **91**, 225.
2 J. B. Torrance, P. Lacorre, A. I. Nazzal, E. J. Ansaldo and Ch. Niedermayer, *Phys. Rev. B*, 1992, **45**, 8209.
3 M. L. Medarde, *J. Phys.: Condens. Matter*, 1997, **9**, 1679.
4 S. J. Kim, G. Demazeau, J. A. Alonso and J. H. Choy, *J. Mater. Chem.*, 2001, **11**, 487.
5 J.-S. Zhou, J. B. Goodenough, B. Dabrowski, P. W. Klamut and Z. Bukowski, *Phys. Rev. Lett.*, 2001, **84**, 526.
6 J. A. Alonso, M. J. Martínez-Lope, M. T. Casais, M. A. G. Aranda and M. T. Fernández-Díaz, *J. Am. Chem. Soc.*, 1999, **121**, 4754.
7 J. A. Alonso, M. J. Martínez-Lope, M. T. Casais, J. L. García-Muñoz and M. T. Fernández-Díaz, *Phys. Rev. B*, 2000, **61**, 1756.
8 J. A. Alonso, M. J. Martínez-Lope, M. T. Casais, J. L. García-Muñoz, M. T. Fernández-Díaz and M. A. G. Aranda, *Phys. Rev. B*, 2001, **64**, 094 102.
9 J. L. García-Muñoz, J. Rodríguez-Carvajal, P. Lacorre and J. B. Torrance, *Phys. Rev. B*, 1992, **46**, 4414.
10 M. Zaghrioui, A. Bulou, P. Lacorre and P. Laffez, *Phys. Rev. B*, 2001, **64**, 081 102.
11 J. Rodríguez-Carvajal, S. Rosenkranz, M. Medarde, P. Lacorre, M. T. Fernández-Díaz, F. Fauth and V. Trounov, *Phys. Rev. B*, 1998, **57**, 456.
12 K. P. Rajeev, N. Y. Vasanthacharya, A. K. Raychauhuri, P. Ganguly and C. N. R. Rao, *Physica C*, 1988, **153–155**, 1331.
13 F. C. Zhang, *Phys. World*, 2001, **14**, 24.
14 Yu. Ya. Tomashpol′skii and Yu. N. Venevtsev, *Izv. Akad. Nauk SSSR, Ser. Neorg. Mater.*, 1967, **3**, 2132.
15 Yu. Ya. Tomashpol′skii, Yu. N. Venevtsev, K. P. Burdina and Yu. N. Venevtsev, *Kristallografiya*, 1968, **13**, 987.
16 Yu. Ya. Tomashpol′skii and Yu. N. Venevtsev, *Izv. Akad. Nauk SSSR, Ser. Neorg. Mater.*, 1969, **5**, 1279.
17 F. Izumi and T. Ikeda, *Mater. Sci. Forum*, 2000, **198**, 321.
18 N. E. Brese and M. O'Keeffe, *Acta Crystallogr., Sect. B*, 1991, **47**, 192.
19 D. E. Cox and A. W. Sleight, *Solid State Commun.*, 1976, **19**, 969.